An HD domain phosphohydrolase active site tailored for oxetanocin-A biosynthesis

Jennifer Bridwell-Rabb[a,b,c], Gyunghoon Kang[b], Aoshu Zhong[d,e], Hung-wen Liu[d,e], and Catherine L. Drennan[a,b,c,1]

[a]Howard Hughes Medical Institute, Massachusetts Institute of Technology, Cambridge, MA 02139; [b]Department of Chemistry, Massachusetts Institute of Technology, Cambridge, MA 02139; [c]Department of Biology, Massachusetts Institute of Technology, Cambridge, MA 02139; [d]Division of Chemical Biology and Medicinal Chemistry, College of Pharmacy, University of Texas at Austin, Austin, TX 78712; and [e]Department of Chemistry, University of Texas at Austin, Austin, TX 78712

Edited by David W. Christianson, University of Pennsylvania, Philadelphia, PA, and accepted by Editorial Board Member Stephen J. Benkovic October 26, 2016 (received for review August 16, 2016)

HD domain phosphohydrolase enzymes are characterized by a conserved set of histidine and aspartate residues that coordinate an active site metallocenter. Despite the important roles these enzymes play in nucleotide metabolism and signal transduction, few have been both biochemically and structurally characterized. Here, we present X-ray crystal structures and biochemical characterization of the *Bacillus megaterium* HD domain phosphohydrolase OxsA, involved in the biosynthesis of the antitumor, antiviral, and antibacterial compound oxetanocin-A. These studies reveal a previously uncharacterized reaction for this family; OxsA catalyzes the conversion of a triphosphorylated compound into a nucleoside, releasing one molecule of inorganic phosphate at a time. Remarkably, this functionality is a result of the OxsA active site, which based on structural and kinetic analyses has been tailored to bind the small, four-membered ring of oxetanocin-A over larger substrates. Furthermore, our OxsA structures show an active site that switches from a dinuclear to a mononuclear metal center as phosphates are eliminated from substrate.

X-ray crystallography | phosphohydrolase | metalloenzymes | natural products | nucleosides

Oxetanocin-A (OXT) is a nucleoside analog produced by *Bacillus megaterium* NK84-0128 (1) that contains an unusual four-membered oxetane ring connected to an adenine base through an *N*-glycosidic linkage (2). Clinical interest in OXT stems from the observed activity against hepatitis B virus (3), herpes simplex virus (1), HIV (4), and human cytomegalovirus (5). This antimicrobial and antiviral activity may be a consequence of the reported inhibition of cellular and viral DNA polymerases by triphosphorylated OXT compounds (6). Four genes located within the *Bgl*II-D fragment (6.8 kb) of the pOXT1 plasmid isolated from the producing strain have been hypothesized to encode proteins involved in OXT production (OxsA and OxsB) and OXT resistance (OxrA and OxrB) (7).

OxsA is a member of the HD domain superfamily of enzymes. This superfamily is divided into classes of enzymes that use a His-Asp doublet of residues and an additional series of conserved His and Asp residues to coordinate a single divalent metal (HX_nHDX_nD motif) (8, 9), a dinuclear metal active site ($HX_nHDX_nHX_nHX_nD$ motif) (10, 11), or a recently described trinuclear iron metal-center (12). Although in many cases the identity of the relevant catalytic metal required for chemistry in vivo is unclear, there are examples of mononuclear enzymes that can use magnesium (13), cobalt (14), or manganese (8, 13, 15), and dinuclear enzymes that can use nickel (16), manganese (17), or iron (10, 18–20).

Most of the biochemically characterized HD domain enzymes catalyze phosphoester bond hydrolysis and are annotated as phosphohydrolases (8, 9). Their reactions are reasonably diverse and include hydrolysis of a phosphate from 2′-deoxyadenosine monophosphate (dAMP) by the *Escherichia coli* enzyme YfbR (14), hydrolysis of pyrophosphate from (p)ppGpp (13) or a deoxyribonucleoside triphosphate (15), and hydrolysis of inorganic triphosphate from deoxyadenosine triphosphate (dATP) (21, 22). These enzymes can also cleave the phosphodiester bond of cyclic-di-GMP (11, 23). Finally, two HD domain enzymes, *myo*-inositol oxygenase and PhnZ, are not hydrolases at all. They bind mixed-valent Fe^{2+}/Fe^{3+} metal centers and operate as oxygenases, indicating the chemical diversity possible with the HD domain fold (10, 18, 20, 24–26).

Here we investigate two plausible mechanistic proposals for the biosynthesis of OXT through the biochemical and structural characterization of OxsA (Fig. 1). In the first proposal, OxsA catalyzes the removal of one or multiple phosphates from a phosphorylated 2′-deoxyadenosine derivative, and OxsB, a cobalamin-dependent *S*-adenosylmethionine (AdoMet) radical enzyme, catalyzes a radical rearrangement to form the oxetane ring of OXT. In the second proposal, OxsB catalyzes ring contraction first, and OxsA works second to hydrolyze one or multiple phosphates from the phosphorylated OXT product.

Results

OxsA Has a Mononuclear HD Domain Phosphohydrolase Fold. The crystal structure of OxsA was determined to 2.05-Å resolution using the E72A variant of the *E. coli* 5′-nucleotidase, YfbR (14), as a search model. The data collection and refinement statistics for all determined structures are listed in Table S1. Similar to the structure of YfbR, OxsA has a globular fold composed of eight

Significance

Over the past few decades, natural products, or chemical compounds derived from plants, animals, or microbes have greatly inspired drug discovery. Because natural products often have more complex and architecturally unique scaffolds than available man-made drugs, characterization of natural product biosynthetic pathways often reveals unprecedented chemistry and enzymatic platforms. Oxetanocin-A (OXT) is a natural product nucleoside analog that has an unusual four-membered oxetane ring connected to an adenine base. Prior to this work, there were no details available about OXT biosynthesis. Here, we not only elucidate a scheme for the two-enzyme catalyzed production of OXT, but also reveal modifications to an HD domain phosphohydrolase enzyme scaffold that expand the catalytic repertoire of this enzyme superfamily.

Author contributions: J.B.-R. and C.L.D. designed research; J.B.-R. and G.K. performed research; J.B.-R. and A.Z. contributed new reagents/analytic tools; J.B.-R., G.K., A.Z., H.-w.L., and C.L.D. analyzed data; and J.B.-R., H.-w.L., and C.L.D. wrote the paper.

The authors declare no conflict of interest.

This article is a PNAS Direct Submission. D.W.C. is a Guest Editor invited by the Editorial Board.

Data deposition: The atomic coordinates and structure factors have been deposited in the Protein Data Bank, www.pdb.org (PDB ID codes 5TK6, 5TK7, 5TK8, 5TK9, and 5TKA).

[1]To whom correspondence should be addressed. Email: cdrennan@mit.edu.

This article contains supporting information online at www.pnas.org/lookup/suppl/doi:10.1073/pnas.1613610113/-/DCSupplemental.

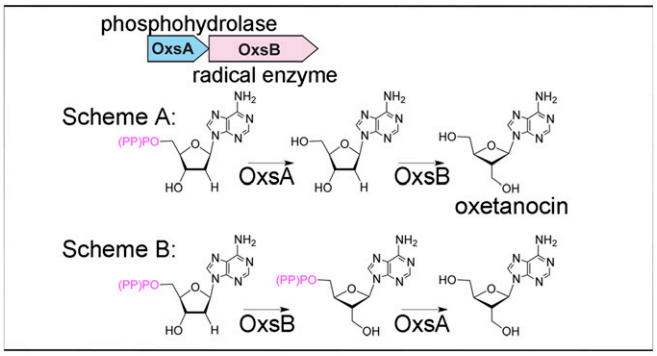

Fig. 1. Proposed schemes for OXT biosynthesis using the proteins encoded by the *oxsA* and *oxsB* production genes, which are annotated as an HD domain phosphohydrolase and a cobalamin-dependent AdoMet radical enzyme, respectively.

α-helices (Fig. 2*A*). There is one monomer of OxsA per asymmetric unit, but based on an approximate 2,600-Å^2 interface (23% of the total monomeric surface area) between the OxsA monomer and a symmetry-related molecule, it appears the biological unit of OxsA is a dimer (Fig. S1). This interface maps to the dimer interface previously identified in YfbR, formed predominantly between α-helices 1 and 3 (14). An active site Mg^{2+} from the crystallization solution is found at the core of the α-helices, octahedrally coordinated by His31, His66, Asp67, and Asp132 of the characteristic HX_nHDX_nD motif, and two water molecules. Residues Met1, Ile76–Ile97, and Arg191–Asn194 were too disordered to build and are therefore missing from the refined structure of OxsA.

Structure of OxsA with Oxetanocin 5′-Monophosphate Reveals a Tailored Active Site Architecture. The structure of OxsA cocrystallized with chemically synthesized oxetanocin-5′-monophosphate ($OxsA^{OXT\text{-}P}$) was determined to 1.64-Å resolution. The structure of $OxsA^{OXT\text{-}P}$ is similar to the ligand-free structure with an rmsd determined by PyMOL of 0.22 Å for 1,014 atoms. The main difference between the ligand-bound structure and the ligand-free structure is the ability to model residues Ile76–Ile97 (Fig. 2*A*). Upon binding OXT-P, these residues order to form a short helical loop following α3 and all of α4, such that only residues 1 and 193–194 are absent from the $OxsA^{OXT\text{-}P}$ structure.

Binding of OXT-P in the active site of OxsA involves interactions between the ε-nitrogen of His75 and the C3′-hydroxymethyl group of OXT, as well as a hydrogen bond between the backbone amide of Ser78 and the endocyclic oxygen of OXT (Fig. 2*B* and Fig. S2*A*). The active site of $OxsA^{OXT\text{-}P}$ is similar to that of YfbR (Fig. 2*C*) and contains previously identified important YfbR residues, including: Trp17 (OxsA numbering), a residue proposed to sterically occlude ribonucleotide binding; Glu70, a residue hypothesized to be involved in protonation of the nucleoside product; and Arg16, which positions the 5′-phosphate of the YfbR substrate, dAMP, for catalysis (14). Consistent with this role, the guanidinium group of Arg16 of OxsA orients the 5′-phosphate of OXT-P near Mg^{2+} and within a positively charged pocket formed by residues Arg16, Lys81, Lys82, Lys87, Arg94, and Lys161 (Fig. 2*B*).

Notably, because OxsA and YfbR share only 30% sequence identity, there are also active site differences. Specifically, His75 of OxsA, the residue that contacts the C3′-hydroxymethyl group of OXT, is a catalytically essential Asp in YfbR (Asp77) (14). The smaller Asp is ideal for accommodating the larger deoxyribose ring of the YfbR substrate (dAMP) and for hydrogen bonding to the 3′-hydroxyl moiety of dAMP. In contrast, the larger His residue in OxsA nicely accommodates the smaller four-membered ring of OXT (Fig. 2*C*) and hydrogen bonds to Glu70, the equivalent of which is the proposed catalytic acid in YfbR (14). Interestingly, although the phosphates of dAMP and OXT-P occupy almost identical active site positions (Fig. 2*C*), the metal positions are slightly different, resulting in direct interaction between dAMP and the closer Co^{2+} in YfbR and a through-water interaction for OXT-P and Mg^{2+} in OxsA. Although this variation may be a result of the difference in the metal that was cocrystallized with the proteins (Mg^{2+} in OxsA or Co^{2+} in YfbR), it should be noted that an inactive E72A-variant was used to determine the structure of Co^{2+}-YfbR with dAMP-bound (14), and that E72 (E70 in OxsA) is very close to the substrate and metal center (Fig. 2*C*). As described below, Co^{2+} may be the catalytic metal in this site for both OxsA and YfbR.

Additional differences in the active site of OxsA and YfbR become evident upon comparison of the electrostatic potential surfaces; the aforementioned positively charged pocket of OxsA appears poised to accommodate one or multiple phosphates (Fig. 2 *B* and *D*). In contrast, the active site of YfbR demonstrates an overall negative charge (Fig. 2*E*) and, consistent with this observation, YfbR lacks activity for deoxyribonucleoside di- and triphosphorylated substrates (14).

OxsA Activity Assays Show Higher in Vitro Activity with Co^{2+} Than Mg^{2+}. The phosphatase activity of OxsA was tested against OXT-P using the malachite green assay, as previously described (27). Briefly, the assay measures activity using the absorbance of the

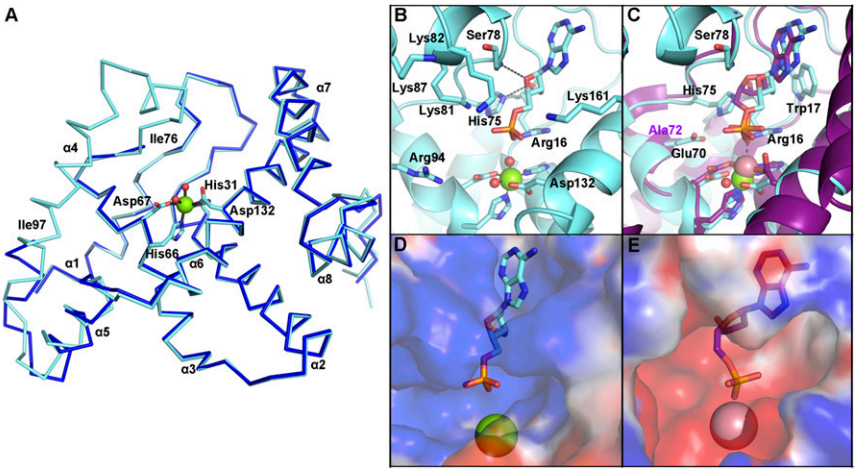

Fig. 2. OxsA has a mononuclear HD domain phosphohydrolase protein fold that appears designed to bind nucleoside analogs with four-membered rings. (*A*) The structure of OxsA (blue) is missing residues Ile76–Ile97, which become ordered in the $OxsA^{OXT\text{-}P}$ structure (cyan). (*B*) OXT-P binds within the HD domain active site and interacts with His75 and the backbone of Ser78. Arg16 orients the 5′-phosphate of OXT-P near Mg^{2+} and within a positively charged pocket. (*C*) Despite sharing similar architectures, an overlay of E72A-YfbR (purple) with bound dAMP reveals that the 3′-carbon of dAMP would be located unfavorably close (1.4 Å) to the ε-nitrogen of His75. (*D*) The overall positive electrostatic potential of the OxsA active site. (*E*) The electrostatic potential measured for the equivalent pocket of E72A-YfbR (14) shows an overall negative charge. In *D* and *E*, the electrostatic potential surfaces are displayed on an equivalent scale. Green and pink spheres represent the divalent metal cocrystallized with OxsA (Mg^{2+}) and E72A-YfbR (Co^{2+}).

BIOCHEMISTRY

complex formed between ammonium molybdate, malachite green, and free inorganic phosphate produced from the hydrolysis reaction. Activity was measured in the presence of Zn^{2+}, Mn^{2+}, Mg^{2+}, or Co^{2+} (Fig. 3). Similar to YfbR, Co^{2+}-OxsA is most active (14, 28), whereas Zn^{2+}-, Mn^{2+}-, and Mg^{2+}-bound OxsA showed lower levels of activity.

Crystal Structures of OxsA with Multiply Phosphorylated OXT Molecules Reveal a Change in the Active Site Metal Content. To investigate whether OxsA is able to bind and turnover multiply phosphorylated OXT molecules, as we predicted above based on the positive electrostatic surface of the OxsA active site, a protocol, which involved the use of the chemically synthesized OXT-P and the commercially available enzymes myokinase and pyruvate kinase, was developed to generate OXT diphosphate (OXT-PP) and OXT triphosphate (OXT-PPP) (Fig. S3). Using this material, the structures of $OxsA^{OXT\text{-}PP}$ and $OxsA^{OXT\text{-}PPP}$ were determined to 1.92- and 1.90-Å resolution, respectively. Similar to the structure of $OxsA^{OXT\text{-}P}$, residues Ile76–Ile97 are ordered and accommodate the bound OXT derivatives. In comparison with the $OxsA^{OXT\text{-}P}$ structure, the rmsds determined by PyMOL for the $OxsA^{OXT\text{-}PP}$ and $OxsA^{OXT\text{-}PPP}$ structures are 0.16 Å for 1,243 atoms and 0.20 Å for 1,184 atoms, respectively.

Surprisingly, despite remarkable similarities in the position of the oxetane ring and adenine base in the active sites of $OxsA^{OXT\text{-}P}$, $OxsA^{OXT\text{-}PP}$, and $OxsA^{OXT\text{-}PPP}$, the structures with OXT-PP and OXT-PPP have a second active site Mg^{2+} (Fig. 4 *A*–*C* and Fig. S2). Because all crystals were grown with the same concentration of Mg^{2+}, the presence of the second Mg^{2+} would seem to be due to the binding of di- and triphosphorylated substrates. As these compounds likely exist in the cell as Mg^{2+}-complexes, OXT-PP and OXT-PPP could deliver the second Mg^{2+} upon binding. Accordingly, the structure of OxsA with OXT bound ($OxsA^{OXT}$), also determined in this work to 1.85-Å resolution, which similar to OXT-P cannot deliver a metal ion to the active site, shows only one Mg^{2+} in the canonical HD-site (Fig. 4*D*).

In the structure of $OxsA^{OXT\text{-}P}$ introduced above, HD residue Asp132 is found bent 2.8 Å toward the active site metal ion and away from the negative charge of the 5′-phosphate of OXT-P, and His66 exhibits two conformations, where in one it serves as a ligand to Mg^{2+} and in the other it is flipped out away from the metal center, replaced by a water molecule (Fig. 4*C*). In contrast, structures with OXT-PP and OXT-PPP show His66 in one conformation, ligating the lower HD-site metal ion of the dinuclear center, and Asp132 serving as a bridging ligand between the two metal ions (Fig. 4 *A* and *B*). The second active site metal ion of the $OxsA^{OXT\text{-}PP}$ structure exhibits an octahedral coordination geometry, coordinated by Asp132, one oxygen atom of each the α- and β- phosphate groups, and three water molecules (Fig. 4*B*). For the $OxsA^{OXT\text{-}PPP}$ structure, the six-coordinate geometry is fulfilled by Asp132, one oxygen atom of each the α-, β-, and γ-phosphate groups, and two water molecules (Fig. 4*A*). The two metal centers are separated by 5.3- and 5.2-Å for the $OxsA^{OXT\text{-}PP}$ and $OxsA^{OXT\text{-}PPP}$ structures, respectively, which is different from other HD domain dinuclear sites, which are separated by 3.4–3.8 Å [PDB ID codes 3TM8 (11), 2IBN (29), 3CCG 2O08, 2OGI, 2PQ7, and 4N6W (18)] and bridged by the HD doublet Asp residue (Fig. 4 *E*–*G*).

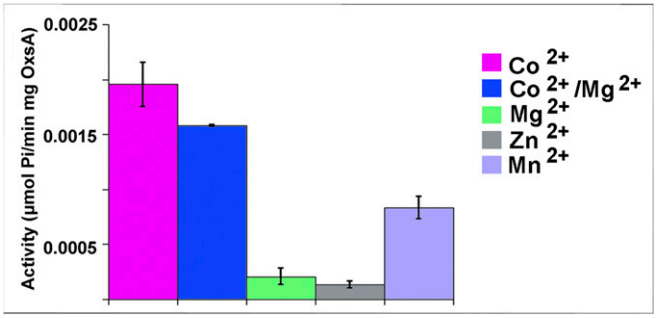

Fig. 3. OxsA activity as measured in the presence of 20 μM OXT-P and 0.6 mM of the indicated divalent metal ions. Co^{2+}-OxsA shows the highest level of activity. Error bars represent ± SD of three independent experiments.

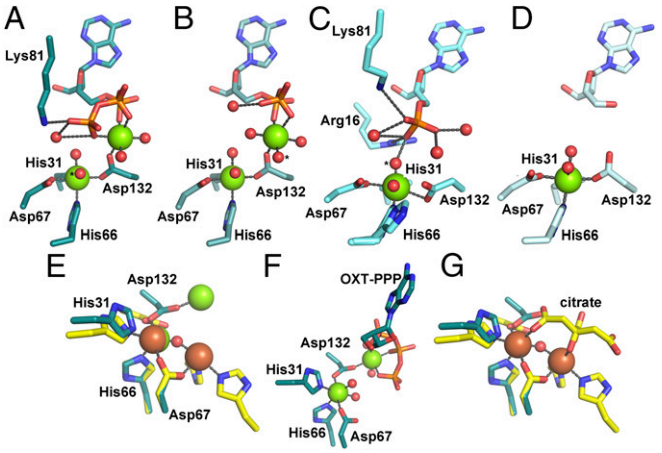

Fig. 4. The metal content of the OxsA active site is modulated through substrate binding. (*A*) $OxsA^{OXT\text{-}PPP}$ has a dinuclear center with one Mg^{2+} found in the HD-site and the other ligated primarily by substrate. (*B*) A similar dinuclear site is observed in $OxsA^{OXT\text{-}PP}$. (*C*) $OxsA^{OXT\text{-}P}$ has a single Mg^{2+} ligated by the mononuclear HD domain residues. His66 exhibits two conformations. (*D*) A mononuclear site is also observed in the structure of $OxsA^{OXT}$. (*E*) Overlay of $OxsA^{OXT\text{-}PPP}$ (dark cyan) with PhnZ (yellow) reveals use of a different Asp as the bridging ligand of the dinuclear site. (*F*) Mg^{2+} in the second site in $OxsA^{OXT\text{-}PPP}$ is 5.2-Å from Mg^{2+} in the HD-site and has only one protein ligand. (*G*) The Fe ions in PhnZ are 3.7 Å apart, bridged by a μ-oxo moiety and a citrate molecule from the crystallization buffer that binds in place of substrate (18). The second Fe site has three protein ligands (18). In *A*–*C*, the proposed nucleophilic water is indicated by an asterisk (*). Green, brown, and red spheres correspond to magnesium, iron, and water molecules, respectively. Stereoviews of $OxsA^{OXT\text{-}P}$, $OxsA^{OXT\text{-}PP}$, and $OxsA^{OXT\text{-}PPP}$ can be found in Fig. S2.

OxsA Shows Activity with Di- and Triphosphorylated OXT. The phosphatase activity of OxsA was tested against OXT-PP, OXT-PPP, 2′-deoxyadenosine diphosphate (dADP), and dATP using the malachite green assay described above. Activity is much lower in the presence of Mg^{2+} compared with Co^{2+} (Fig. 5*A*), explaining why we did not observe turnover in our crystals. As mentioned above, capturing the structure of YfbR with substrate and Co^{2+} required use of inactive mutant protein. Interestingly, a 50:50 Mg^{2+}/Co^{2+} mixture does not reduce the activity compared with 100% Co^{2+} (Fig. 5*A*), suggesting that the highest level of activity requires Co^{2+} to be present in only one of the two metal sites.

The k_{cat} of OxsA with OXT-PPP and OXT-PP was 3.8- and 2.4-fold higher, respectively, than was measured with OXT-P (Table 1). This trend is reflective of what is observed in solution; phosphate esters are more stable to hydrolysis than phosphoanhydrides. Thus, it does not appear that OxsA has evolved to be a much better catalyst for one of the phosphorylated forms of OXT over another. The K_M values are similar for all three phosphorylated forms of OXT, and are between 8 and 13 μM (Table 1). Therefore, for the OXT molecules, each added phosphate equates to an increase in the k_{cat} of OxsA and a corresponding increase in the k_{cat}/K_M. The same is not true for the phosphorylated deoxyadenosine substrates, for which OxsA activity on dADP was lower than for both dATP and dAMP (Fig. 5*A* and Table 1). This difference could be due in part to the fact that the commercially available deoxyribonucleotide compounds are less pure (98–100%, ≥95%,

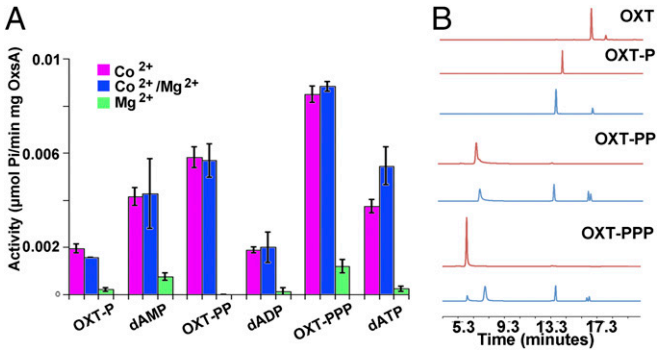

Fig. 5. OxsA activity on phosphorylated OXT and deoxyadenosine compounds. (*A*) The activity of OxsA is plotted as a function of tested substrate (10 molar equivalents) in the presence of Co^{2+}, Mg^{2+}, or a Co^{2+}/Mg^{2+} mixture. Error bars represent the ± SD of three independent experiments. (*B*) HPLC analysis of OxsA hydrolysis products when incubated with OXT derivatives (OXT-PPP, OXT-PP, or OXT-P). Each red trace corresponds to an OXT derivative standard. The blue traces correspond to hydrolysis products after incubation of the OXT derivative with OxsA. Current LC-MS data indicates splitting of the nucleoside peak is because of hydroxylation that occurs under the HPLC assay conditions.

and ≥97% purity for dAMP, dADP, and dATP, respectively) than both our chemically and enzymatically synthesized OXT standards. Importantly, the K_M values for dAMP, dADP, and dATP are 2- to 20-fold higher (22–155 μM) than the K_M values for OXT-P(PP) (Table 1). In the case of dATP (155 ± 18 μM), the K_M is almost equivalent to what has previously been measured as the concentration in bacterial cells (175–200 μM) (30, 31), indicating OxsA is not a good catalyst for dATP hydrolysis.

A similar study of activity was pursued using HPLC to investigate production of OXT and deoxyribonucleotide hydrolysis products. In both cases, the diphosphate, monophosphate, and nucleoside products were detected consistent with OxsA being able to release more than one molecule of phosphate from the provided substrates until the nucleoside products, OXT or 2′-deoxyadeonosine, are produced (Fig. 5*B* and Fig. S4).

The observed substrate tolerance of OxsA prompted an investigation into the B-factors of the OxsA structures with OXT molecules bound. Within each determined structure, similar B-factors are observed in the core helices (α1–α3, and α6), which contribute the HD-metal binding residues. The highest B-factors are found on the loop following the His75 helix, and on α4-α5 (Fig. S5). Both His75 and Ser78, which form the two principle interactions with all OXT derivatives in the active site, fall in a region where the average B-factor is 10–15 $Å^2$ higher than the average for the entire structure. This flexibility likely allows for nonoptimal substrates to be accommodated in the active site, albeit giving rise to higher K_M values. Unfortunately, molecular details of this accommodation are not available, as crystals grown or soaked with a 5- to 100-fold molar excess of the deoxyribonucleotide molecules do not reveal any electron density for bound ligands.

Discussion

To study the mechanism by which OxsA and OxsB catalyze the synthesis of OXT, we have determined the structures of five states of OxsA ($OxsA^{OXT\text{-}PPP}$, $OxsA^{OXT\text{-}PP}$, $OxsA^{OXT\text{-}P}$, $OxsA^{OXT}$, and OxsA) using X-ray crystallography. These structural studies coupled with the malachite green assay of detecting inorganic phosphate production, the Michaelis–Menten kinetic measurements, and the HPLC analysis of hydrolysis product formation are consistent with the proposed scheme B for OXT biosynthesis (shown in Fig. 1). In this scheme, OxsA catalyzes the hydrolysis of a phosphorylated OXT molecule to generate the nucleoside product of the pathway.

Because of the simple nature of the OXT biosynthetic gene cluster, first contracting the more thermodynamically stable five-membered ring of a purine nucleoside coopted from a primary metabolic pathway to generate the strained, four-membered ring of OXT, followed by dephosphorylation of an OXT phosphate may serve as a mechanism to trap the OXT product and thus prevent its OxsB-catalyzed equilibration with a purine nucleoside phosphate. Interestingly, it appears that regardless of whether dAMP, dADP, or dATP is contracted by OxsB, OxsA can catalyze hydrolysis of the resultant OXT-derivative down to OXT, one phosphate at a time. The K_M values for each of the OXT derivatives are similar, potentially allowing OxsA to hold on to the phosphorylated forms of OXT until final conversion to OXT is achieved. From the perspective of chemical warfare between microbes, the phosphorylated forms of OXT are likely the toxic species. Indeed, OXT-PPP has been shown to inhibit cellular and viral DNA polymerases (6). Therefore, it appears that the combined action of OxsA and OxsB generate the warfare agent, OXT, but renders the compound inert for transport out of the cell. Consequently, OxsA can be thought of as having a dual function: OxsA is involved in both completing the biosynthesis of OXT and imparting resistance to the producing strain. Presumably, OXT is then taken up by a neighboring organism and rephosphorylated, thus reacquiring its toxicity. In line with this theory are our results that promiscuous kinases can be used to enzymatically generate OXT-PP and OXT-PPP with reasonable yields.

The X-ray crystal structures of OxsA presented in this work add another level of diversity to the HD domain superfamily; the active site appears to be designed to bind the secondary metabolite OXT and also decrease the binding affinity of substrates with larger deoxyribose rings. This design is accomplished by the use of a bulky His residue near the HD-active site metal ion in place of the equivalent Asp found in YfbR. Notably, however, this enzyme redesign places His75 in a highly flexible region of the protein, which when not bound with OXT, affords enzymatic promiscuity, allowing hydrolysis of deoxyribonucleotide substrates, albeit with lower catalytic efficiency (a consequence of the presumed decrease in substrate affinity illustrated by the measured K_M values).

Table 1. Summary of kinetic parameters for OxsA with OXT- and deoxyribonucleotide compounds

Tested substrate	K_M (μM)	$V_{max} \times 10^{-3}$ (U/mg)*	$k_{cat} \times 10^{-3}$ (s^{-1})	k_{cat}/K_M ($M^{-1}\cdot s^{-1}$)
OXT-P	11 ± 3	3.2 ± 0.20	1.2 ± 0.077	106 ± 30
dAMP	22 ± 2	9.8 ± 0.24	3.7 ± 0.094	167 ± 16
OXT-PP	13 ± 3	7.8 ± 0.46	2.9 ± 0.17	221 ± 47
dADP	53 ± 11	7.1 ± 0.35	2.6 ± 0.13	51 ± 10
OXT-PPP	8 ± 2	12 ± 0.86	4.5 ± 0.33	525 ± 121
dATP	155 ± 18	58 ± 2.4	22 ± 0.83	142 ± 17

See *SI Materials and Methods* for experimental details.
*U/mg = μmol/min mg of OxsA.

The enzyme YedJ, which also has a His residue in the equivalent position, similarly shows poor activity with primary metabolic phosphatase and phosphodiesterase substrates (14).

Perhaps even more impressive is the revelation from this structural work that an HD domain scaffold can accommodate more than one type of metal center depending on which substrate is bound. Before this work, there were characterized HD domain enzymes, which use mono- (14, 15, 21, 22, 32, 33), di- (10, 11, 16–18, 23, 24, 29, 34), and trinuclear (12) metal centers, but no examples that use "switchable" metallocenters nor examples of dinuclear sites that resemble the one that we observe here. We hypothesize that this second metal center is introduced as a consequence of binding a Mg^{2+}-OXT di- or triphosphate molecule. As discussed below, the use of a second metal site extends the hydrolytic capabilities of the active site, allowing OxsA to catalyze three-phosphate elimination reactions at the α-, β-, and γ-positions of its substrate. The observed mono- to di-nuclear metal switching mechanism of OxsA is vaguely reminiscent of RNA polymerase II, which requires two Mg^{2+} ions that are bridged by an Asp and located 5.8 Å apart; one Mg^{2+} remains bound to the enzyme and one Mg^{2+} is only stably bound in the presence of a nucleotide substrate (35, 36). Unlike OxsA, however, in RNA polymerase II the stable Mg^{2+} has three Asp ligands and coordinates the α-phosphate of the substrate, and the transient Mg^{2+} has additional protein ligands (35, 36).

Mechanistically, the vast majority of phosphate elimination reactions proceed through an in-line attack by a nucleophile, at the phosphorus atom, opposite the position of the leaving group (37). This type of reaction is one proposal for YfbR, where hydrolysis requires that the 5′-phosphate of dAMP coordinates the HD-metal center, and is thereby positioned for nucleophilic attack by a Co^{2+} bound hydroxide ion, followed by, or with concomitant protonation of the leaving group by Glu72 (Glu70 in OxsA numbering) (14). Based on the X-ray crystal structures determined here, it can be intuited how OxsA could use a similar mechanism to catalyze three sequential hydrolysis reactions with the involvement of three different water molecules (starred in Fig. 4) and a flexible dinuclear motif that has only one protein-based ligand to the second metal ion.

With respect to hydrolysis of the γ-phosphate of OXT-PPP, a water molecule bound to the metal ion in the canonical HD-site is positioned correctly to serve as the nucleophile (Fig. 4*A*). Metal ions act as Lewis acids, lowering the pK_a of bound water molecules and activating them for nucleophilic attack on phosphorylated compounds. For hydrolysis of the β-phosphate, a water molecule bound to the metal ion in the noncanonical site meets the requisite geometric requirement (Fig. 4*B*). Accordingly, even if this second metal ion binds as part of the substrate, the active site does require its presence for hydrolysis of OXT-PP. Loss of this second metal site is expected to occur along with or following hydrolysis of the β-phosphate. The remaining phosphate of OXT-P moves down to occupy the second metal site, repositioning Asp132 (Fig. S6*A*). An exit route for the metal ion can be visualized in a surface representation of the dinuclear OxsA protein, which reveals that the second site is much more solvent accessible than the HD-site (Fig. S6*B*) as well as a typical HD domain second metal site (Fig. S7).

In part because of the transient nature of the second metal site in OxsA, we propose that Mg^{2+} and not Co^{2+} is the relevant noncanonical metal in vivo. Our data show that Co^{2+}-OxsA and Co^{2+}/Mg^{2+}-OxsA have similarly high levels of activity, indicating that Co^{2+} need not occupy both sites for maximum turnover. Additionally, Co^{2+} decreases cellular growth rate and becomes toxic to *B. megaterium* at levels above 50 μM (38), whereas Mg^{2+} is typically present in the millimolar range in cells (39) and commonly associated with phosphorylated molecules. Although it is possible that the physiologically relevant metal in both sites is Mg^{2+}, *B. megaterium* is a major producer of cobalamin (40), requiring a cellular flux of Co^{2+} that should be sufficient to fill a canonical and stable metal site. For these reasons, we suggest that the dinuclear site is composed of Co^{2+} in the canonical HD-site and Mg^{2+} in the noncanonical, transient secondary site, which is introduced with OXT-PP and OXT-PPP substrates.

Finally, for hydrolysis of the α-phosphate, a water bound to the metal in the HD-site is positioned appropriately (3.6 Å from the phosphorus atom) (Fig. 4*C*). In addition to metal-catalyzed water activation, the enzymatic mechanism may involve modulation of the electrophilicity of the phosphate to be hydrolyzed, as our structures show an overall positive active site electrostatic potential (Fig. 2*D*) created by a number of Lys and Arg residues in addition to the metal ions that are present (Fig. 2*C*).

Although OxsA appears tailored to perform hydrolysis reactions on three different forms of the secondary metabolite OXT, likely using three different water molecules bound to metal ions in two different metal-binding sites, OxsA is neither highly specific nor highly active. For example, the specific activity of Co^{2+}-OxsA is ∼85 times slower than that observed for YfbR with its native substrate dAMP (14). Even though primary metabolic enzymes are often faster than ones involved in secondary metabolism, OxsA rates of 0.0012–0.022 s^{-1} (0.072–1.3 min^{-1}) (Table 1) still seem modest. Although turnover numbers for OxsA's partner enzyme, OxsB, have not yet been reported, AdoMet radical enzymes are notoriously slow. A recent review article reports that rates are typically on the order of 0.018–1.6 min^{-1} (41). If OxsB turns out to be a typical AdoMet radical enzyme, it seems likely that there would have been little evolutionary pressure to evolve OxsA to turn over phosphorylated OXT molecules much faster than they are being produced. A biochemical characterization of OxsB will be informative in this regard.

There are currently ∼100,000 protein X-ray crystal structures deposited in the PDB. Despite this large number, it has been estimated that fewer than 1,000 unique protein folds exist (42). This discrepancy means that protein scaffolds must be reused and reinvented for new catalytic functions through divergent or convergent evolution (8, 43). One theory for how Nature repurposes protein architectures is that it selects from a pool of enzymes with mechanisms that would lend a strategy for catalysis of a new reaction (43). Often, this approach is at the expense of a lower enzymatic rate and catalytic promiscuity for the original substrate (43). Similar to the production of OXT, a toxic compound, the redesign of an enzyme has the ability to give the host a competitive advantage (43). These concepts are exemplified by the HD domain enzyme superfamily whose catalytic repertoire is just starting to be unveiled. Here, we report a customized HD domain active site architecture and a switchable metallocenter, which is regulated by the binding of OXT substrates. These studies reveal the function of OxsA and serve to elucidate a scheme for a two-enzyme catalyzed biosynthesis of the nucleoside analog OXT.

Materials and Methods

The *oxsA* gene was synthesized by Mr. Gene with codon optimization for *E. coli* expression, subcloned into the pET24b(+) vector, and transformed into *E. coli* BL21-star-(DE3). OxsA was purified using ammonium sulfate precipitation and a DEAE-Sepharose CL-6B column. OXT and OXT-P were chemically synthesized (Scheme S1), whereas OXT-PP and OXT-PPP were enzymatically generated. Inorganic phosphate production was measured using the absorbance of malachite green at 630 nm (27). The OxsA reaction products were detected at 260 nm following separation on an analytical C-18 reverse-phase HPLC column. The structure of OxsA was solved using the structure of YfbR (14) as a molecular replacement model. The structure of OxsA was used to determine the structure of $OxsA^{OXT}$, which was used to determine the structures of $OxsA^{OXT\text{-}P}$, $OxsA^{OXT\text{-}PP}$, and $OxsA^{OXT\text{-}PPP}$. Detailed protocols can be found in *SI Materials and Methods*.

ACKNOWLEDGMENTS. This work was supported by National Institute of Health Grants F32-GM108189 (to J.B.-R.) and GM035906 (to H.-w.L.), and Welch Foundation Grant F-1511 (to H.-w.L.). C.L.D. is a Howard Hughes Medical Institute Investigator. This work is based upon research conducted at the

Northeastern Collaborative Access Team beamlines, which are funded by the National Institute of General Medical Sciences from the National Institutes of Health (P41 GM103403). The Pilatus 6M detector on 24-ID-C beam line is funded by a NIH-Office of Research Infrastructure Programs High-End Instrumentation Grant S10 RR029205. This research used resources of the Advanced Photon Source, a US Department of Energy (DOE) Office of Science User Facility operated for the DOE Office of Science by Argonne National Laboratory under Contract DE-AC02-06CH11357. This work also includes research conducted at the Stanford Synchrotron Radiation Lightsource. Use of the Stanford Synchrotron Radiation Lightsource, SLAC National Accelerator Laboratory, is supported by the US DOE, Office of Science, Office of Basic Energy Sciences under Contract DE-AC02-76SF00515. The Stanford Synchrotron Radiation Lightsource Structural Molecular Biology Program is supported by the DOE Office of Biological and Environmental Research, and by the National Institutes of Health, National Institute of General Medical Sciences (including P41GM103393).

1. Shimada N, et al. (1986) Oxetanocin, a novel nucleoside from bacteria. *J Antibiot (Tokyo)* 39(11):1623–1625.
2. Nakamura H, et al. (1986) The X-ray structure determination of oxetanocin. *J Antibiot (Tokyo)* 39(11):1626–1629.
3. Ueda K, Tsurimoto T, Nagahata T, Chisaka O, Matsubara K (1989) An in vitro system for screening anti-hepatitis B virus drugs. *Virology* 169(1):213–216.
4. Hoshino H, Shimizu N, Shimada N, Takita T, Takeuchi T (1987) Inhibition of infectivity of human immunodeficiency virus by oxetanocin. *J Antibiot (Tokyo)* 40(7):1077–1078.
5. Nishiyama Y, Yamamoto N, Takahash K, Shimada N (1988) Selective inhibition of human cytomegalovirus replication by a novel nucleoside, oxetanocin G. *Antimicrob Agents Chemother* 32(7):1053–1056.
6. Izuta S, et al. (1992) Inhibitory effects of triphosphate derivatives of oxetanocin G and related compounds on eukaryotic and viral DNA polymerases and human immunodeficiency virus reverse transcriptase. *J Biochem* 112(1):81–87.
7. Morita M, et al. (1999) Cloning of oxetanocin A biosynthetic and resistance genes that reside on a plasmid of *Bacillus megaterium* strain NK84-0128. *Biosci Biotechnol Biochem* 63(3):563–566.
8. Galperin MY, Koonin EV (2012) Divergence and convergence in enzyme evolution. *J Biol Chem* 287(1):21–28.
9. Aravind L, Koonin EV (1998) The HD domain defines a new superfamily of metal-dependent phosphohydrolases. *Trends Biochem Sci* 23(12):469–472.
10. Brown PM, et al. (2006) Crystal structure of a substrate complex of myo-inositol oxygenase, a di-iron oxygenase with a key role in inositol metabolism. *Proc Natl Acad Sci USA* 103(41):15032–15037.
11. Lovering AL, Capeness MJ, Lambert C, Hobley L, Sockett RE (2011) The structure of an unconventional HD-GYP protein from Bdellovibrio reveals the roles of conserved residues in this class of cyclic-di-GMP phosphodiesterases. *MBio* 2(5):e00163-11.
12. Bellini D, et al. (2014) Crystal structure of an HD-GYP domain cyclic-di-GMP phosphodiesterase reveals an enzyme with a novel trinuclear catalytic iron centre. *Mol Microbiol* 91(1):26–38.
13. Heinemeyer EA, Richter D (1977) In vitro degradation of guanosine tetraphosphate (ppGpp) by an enzyme associated with the ribosomal fraction from *Escherichia coli*. *FEBS Lett* 84(2):357–361.
14. Zimmerman MD, Proudfoot M, Yakunin A, Minor W (2008) Structural insight into the mechanism of substrate specificity and catalytic activity of an HD-domain phosphohydrolase: The 5′-deoxyribonucleotidase YfbR from *Escherichia coli*. *J Mol Biol* 378(1): 215–226.
15. Jeon YJ, et al. (2016) Structural and biochemical characterization of bacterial YpgQ protein reveals a metal-dependent nucleotide pyrophosphohydrolase. *J Struct Biol* 195(1):113–122.
16. Yakunin AF, et al. (2004) The HD domain of the *Escherichia coli* tRNA nucleotidyltransferase has 2′,3′-cyclic phosphodiesterase, 2′-nucleotidase, and phosphatase activities. *J Biol Chem* 279(35):36819–36827.
17. Sultan SZ, et al. (2011) Analysis of the HD-GYP domain cyclic dimeric GMP phosphodiesterase reveals a role in motility and the enzootic life cycle of *Borrelia burgdorferi*. *Infect Immun* 79(8):3273–3283.
18. Wörsdörfer B, et al. (2013) Organophosphonate-degrading PhnZ reveals an emerging family of HD domain mixed-valent diiron oxygenases. *Proc Natl Acad Sci USA* 110(47): 18874–18879.
19. Miner KD, Klose KE, Kurtz DM, Jr (2013) An HD-GYP cyclic di-guanosine monophosphate phosphodiesterase with a non-heme diiron-carboxylate active site. *Biochemistry* 52(32):5329–5331.
20. Xing G, et al. (2006) A coupled dinuclear iron cluster that is perturbed by substrate binding in myo-inositol oxygenase. *Biochemistry* 45(17):5393–5401.
21. Goldstone DC, et al. (2011) HIV-1 restriction factor SAMHD1 is a deoxynucleoside triphosphate triphosphohydrolase. *Nature* 480(7377):379–382.
22. Vorontsov II, et al. (2011) Characterization of the deoxynucleotide triphosphate triphosphohydrolase (dNTPase) activity of the EF1143 protein from Enterococcus faecalis and crystal structure of the activator-substrate complex. *J Biol Chem* 286(38): 33158–33166.
23. Ryan RP, et al. (2006) Cell-cell signaling in *Xanthomonas campestris* involves an HD-GYP domain protein that functions in cyclic di-GMP turnover. *Proc Natl Acad Sci USA* 103(17):6712–6717.
24. Bollinger JM, Jr, Diao Y, Matthews ML, Xing G, Krebs C (2009) myo-Inositol oxygenase: A radical new pathway for O(2) and C-H activation at a nonheme diiron cluster. *Dalton Trans* (6):905–914.
25. McSorley FR, et al. (2012) PhnY and PhnZ comprise a new oxidative pathway for enzymatic cleavage of a carbon-phosphorus bond. *J Am Chem Soc* 134(20):8364–8367.
26. Xing G, et al. (2006) Oxygen activation by a mixed-valent, diiron(II/III) cluster in the glycol cleavage reaction catalyzed by myo-inositol oxygenase. *Biochemistry* 45(17):5402–5412.
27. Baykov AA, Evtushenko OA, Avaeva SM (1988) A malachite green procedure for orthophosphate determination and its use in alkaline phosphatase-based enzyme immunoassay. *Anal Biochem* 171(2):266–270.
28. Proudfoot M, et al. (2004) General enzymatic screens identify three new nucleotidases in *Escherichia coli*. Biochemical characterization of SurE, YfbR, and YjjG. *J Biol Chem* 279(52):54687–54694.
29. Thorsell AG, et al. (2008) Structural and biophysical characterization of human myo-inositol oxygenase. *J Biol Chem* 283(22):15209–15216.
30. Buckstein MH, He J, Rubin H (2008) Characterization of nucleotide pools as a function of physiological state in *Escherichia coli*. *J Bacteriol* 190(2):718–726.
31. Bochner BR, Ames BN (1982) Complete analysis of cellular nucleotides by two-dimensional thin layer chromatography. *J Biol Chem* 257(16):9759–9769.
32. Kondo N, et al. (2007) Structure of dNTP-inducible dNTP triphosphohydrolase: Insight into broad specificity for dNTPs and triphosphohydrolase-type hydrolysis. *Acta Crystallogr D Biol Crystallogr* 63(Pt 2):230–239.
33. Hogg T, Mechold U, Malke H, Cashel M, Hilgenfeld R (2004) Conformational antagonism between opposing active sites in a bifunctional RelA/SpoT homolog modulates (p)ppGpp metabolism during the stringent response [corrected]. *Cell* 117(1):57–68. Erratum in Cell (2004) 117(3):415.
34. van Staalduinen LM, et al. (2014) Crystal structure of PhnZ in complex with substrate reveals a di-iron oxygenase mechanism for catabolism of organophosphonates. *Proc Natl Acad Sci USA* 111(14):5171–5176.
35. Cramer P, Bushnell DA, Kornberg RD (2001) Structural basis of transcription: RNA polymerase II at 2.8 angstrom resolution. *Science* 292(5523):1863–1876.
36. Westover KD, Bushnell DA, Kornberg RD (2004) Structural basis of transcription: Nucleotide selection by rotation in the RNA polymerase II active center. *Cell* 119(4): 481–489.
37. Frey PA (1982) Stereochemistry of enzymatic-reactions of phosphates. *Tetrahedron* 38(11):1541–1567.
38. Moore SJ, Mayer MJ, Biedendieck R, Deery E, Warren MJ (2014) Towards a cell factory for vitamin B12 production in *Bacillus megaterium*: Bypassing of the cobalamin riboswitch control elements. *N Biotechnol* 31(6):553–561.
39. Sissi C, Palumbo M (2009) Effects of magnesium and related divalent metal ions in topoisomerase structure and function. *Nucleic Acids Res* 37(3):702–711.
40. Raux E, Lanois A, Warren MJ, Rambach A, Thermes C (1998) Cobalamin (vitamin B12) biosynthesis: Identification and characterization of a *Bacillus megaterium* cobI operon. *Biochem J* 335(Pt 1):159–166.
41. Broderick JB, Duffus BR, Duschene KS, Shepard EM (2014) Radical S-adenosylmethionine enzymes. *Chem Rev* 114(8):4229–4317.
42. Wolf YI, Grishin NV, Koonin EV (2000) Estimating the number of protein folds and families from complete genome data. *J Mol Biol* 299(4):897–905.
43. Gerlt JA, Babbitt PC (2001) Divergent evolution of enzymatic function: mechanistically diverse superfamilies and functionally distinct suprafamilies. *Annu Rev Biochem* 70:209–246.
44. Norbeck DW, Kramer JB (1988) Synthesis of (-)-Oxetanocin. *J Am Chem Soc* 110(21): 7217–7218.
45. Otwinowski Z, et al. (1997) Processing of X-ray diffraction data collected in oscillation mode. *Methods Enzymol* 276:307–326.
46. Bunkóczi G, Read RJ (2011) Improvement of molecular-replacement models with Sculptor. *Acta Crystallogr D Biol Crystallogr* 67(Pt 4):303–312.
47. Adams PD, et al. (2010) PHENIX: A comprehensive Python-based system for macromolecular structure solution. *Acta Crystallogr D Biol Crystallogr* 66(Pt 2): 213–221.
48. Emsley P, Cowtan K (2004) Coot: Model-building tools for molecular graphics. *Acta Crystallogr D Biol Crystallogr* 60(Pt 12 Pt 1):2126–2132.
49. Moriarty NW, Grosse-Kunstleve RW, Adams PD (2009) Electronic Ligand Builder and Optimization Workbench (eLBOW): A tool for ligand coordinate and restraint generation. *Acta Crystallogr D Biol Crystallogr* 65(Pt 10):1074–1080.
50. Morin A, et al. (2013) Collaboration gets the most out of software. *eLife* 2:e01456.
51. Sali A, Blundell TL (1993) Comparative protein modelling by satisfaction of spatial restraints. *J Mol Biol* 234(3):779–815.
52. Dolinsky TJ, et al. (2007) PDB2PQR: Expanding and upgrading automated preparation of biomolecular structures for molecular simulations. *Nucleic Acids Res* 35(Web Server issue):W522–525.
53. Dolinsky TJ, Nielsen JE, McCammon JA, Baker NA (2004) PDB2PQR: An automated pipeline for the setup of Poisson-Boltzmann electrostatics calculations. *Nucleic Acids Res* 32(Web Server issue):W665–667.
54. Baker NA, Sept D, Joseph S, Holst MJ, McCammon JA (2001) Electrostatics of nanosystems: Application to microtubules and the ribosome. *Proc Natl Acad Sci USA* 98(18): 10037–10041.